

# MaskDiff: Modeling Mask Distribution with Diffusion Probabilistic Model for Few-Shot Instance Segmentation

Minh-Quan Le<sup>1, 2</sup>, Tam V. Nguyen<sup>3</sup>, Trung-Nghia Le<sup>1, 2</sup>, Thanh-Toan Do<sup>4</sup>  
Minh N. Do<sup>5</sup>, and Minh-Triet Tran<sup>1, 2, 6</sup>

<sup>1</sup> University of Science, Ho Chi Minh City, Vietnam

<sup>2</sup> Vietnam National University, Ho Chi Minh City, Vietnam

<sup>3</sup> University of Dayton, United States

<sup>4</sup> Monash University, Australia

<sup>5</sup> University of Illinois at Urbana-Champaign, United States

<sup>6</sup> John von Neumann Institute, Ho Chi Minh City, Vietnam

## Abstract

Few-shot instance segmentation extends the few-shot learning paradigm to the instance segmentation task, which tries to segment instance objects from a query image with a few annotated examples of novel categories. Conventional approaches have attempted to address the task via prototype learning, known as point estimation. However, this mechanism is susceptible to noise and suffers from bias due to a significant scarcity of data. To overcome the disadvantages of the point estimation mechanism, we propose a novel approach, dubbed MaskDiff, which models the underlying conditional distribution of a binary mask, which is conditioned on an object region and  $K$ -shot information. Inspired by augmentation approaches that perturb data with Gaussian noise for populating low data density regions, we model the mask distribution with a diffusion probabilistic model. In addition, we propose to utilize classifier-free guided mask sampling to integrate category information into the binary mask generation process. Without bells and whistles, our proposed method consistently outperforms state-of-the-art methods on both base and novel classes of the COCO dataset while simultaneously being more stable than existing methods.

## 1. Introduction

To achieve outstanding performances, instance segmentation models [11, 3, 18] require to be trained on substantial pixel-level annotated images, which is labor-intensive and costly. Moreover, their ability to generalize from a few examples is still far from acceptable compared to the human visual system, which constrains their feasibility in practical applications. Inspired by the miraculous ability of the hu-

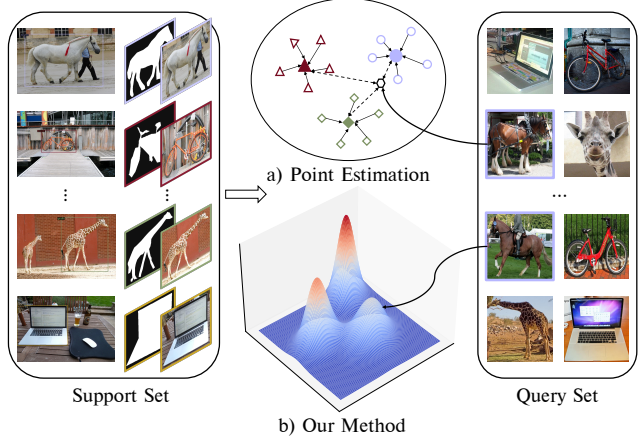


Figure 1. (a) Prior work estimates a specific point as representative of each class [7]. (b) Our MaskDiff method models conditional distribution of masks given object regions and  $K$ -shot samples.

man visual system to recognize novel objects with limited data, few-shot learning (FSL) aims to learn new concepts on a handful of training data ( $K$  examples) by generalizing models trained on base classes to adapt novel classes.

Conventional few-shot instance segmentation (FSIS) methods attempted to address learning on a few examples via prototype learning [7, 8]. This matching mechanism searches the nearest prototype and its corresponding support class from support images as guidance for segmenting the query image (see Fig.1a). Different from existing FSIS methods, we introduce a novel probabilistic model to estimate the distribution of a binary mask given a detected object region and  $K$  samples (see Fig.1b). Concretely, object region, object category, and  $K$ -shot examples are treated as conditional information for generating

the binary mask representation of each object. Mathematically, we model the conditional distribution of a binary mask of an object instance conditioned on an object region and  $K$ -shot knowledge from a specific class  $i$ -th  $p_\theta(y_{\text{mask}} | x_{\text{region}}, K\text{-shot}^i)$ . To the best of our knowledge, our work is the first method to model mask distribution for FSIS.

Derived from the insight which perturbs data with Gaussian noise for populating low data density regions [31] and motivated by diffusion-based models [30, 13], in this paper, we define a Markov chain of diffusion steps to slowly add Gaussian noise to an object mask and then learn to reverse the diffusion process conditioned on an object region and  $K$ -shot samples to reconstruct the desired mask representation corresponding to the objects from the noise. We also design a method using a classifier-free guidance to guide the diffusion model during sampling. Hence, the diffusion model is aware of categories of binary masks in the sampling procedure.

Our proposed approach includes several advantages. First, our method is robust to noise, which is actually the error in few given annotations, and eliminates the bias of the conventional point estimation mechanism since we capture the underlying conditional distribution of mask representation. In the point estimation approach, models depend on prototypes for prediction. If the information provided by prototypes is poor (e.g., few and bad samples), the models will be biased by prototypes. By utilizing diffusion probabilistic model (DPM), a class of deep likelihood-based generative models, we analyze the way to estimate the mask distribution of objects dependent on detected regions and information from  $K$ -shot samples. In addition, we argue that the mask representation is reliant on not only the instance object region but also its category. Therefore, we follow class-specific mask predictor and integrate category knowledge into the mask generation process. Last but not least, our class-specific mask predictor alleviates spatial information losses from pooling operators of existing FSIS methods [8, 25]. When exploiting detected bounding box locations as inputs for diffusion models, we do not leverage any pooled features as Mask-RCNN [11] to generate masks but directly use image channels, thus preserving detailed spatial information. Our contributions lie in four-fold:

- We introduce a novel mask distribution modeling approach, dubbed **MaskDiff**, for FSIS. Conceptually, unlike point estimation, MaskDiff tries to model the conditional distribution of a binary mask conditioned on the detected object region and  $K$ -shot samples.
- Our work is the first one to adapt conditional diffusion probabilistic models for modeling instance binary mask distribution in FSIS.
- We propose to utilize guidance from the available classification head of object detector to integrate cate-

gory information into the mask sampling procedure. Consequently, in the reverse process, the diffusion model is aware of the categories of mask representation. Our class-specific mask predictor outperforms class-agnostic ones [8, 25]. Moreover, when we integrate category information into the mask-generation process, the sampling procedure becomes more stable and produces more organized content.

- Extensive experimental results on the standard COCO dataset show that our MaskDiff not only outperforms state-of-the-art FSIS methods on both base and novel classes but also is more stable than existing methods.

## 2. Related work

**Few-shot instance segmentation (FSIS).** The majority of prior works for FSIS try to provide guidance to specific components of Mask-RCNN [11] to guarantee that the networks better understand novel classes or both base and novel classes as well. FGN [7] integrates multiple guiding techniques into the core components of Mask R-CNN [11], such as masked pooling operator is applied before computing the class-attentive vectors and generating masks. Most early approaches adapted meta-learning to episodic training [23, 35, 7]. Following this training direction, few modern methods utilized anchor-free object detectors to directly segment objects from arbitrary categories given by reference images [24, 33]. On the other hand, Wang *et al.* [34] proposed a two-stage fine-tuning approach (TFA) which first trains Faster-RCNN [27] on the base classes and then fine-tunes the box predictor on a balanced subset of base and novel classes. Modern FSIS methods [34, 8, 25] were then developed in this fine-tuning direction by fine-tuning the last layers of certain heads on novel classes. Our proposed MaskDiff also follows the latter training strategy. In addition, current techniques [8, 25] mainly concentrate on class-agnostic mask prediction heads, which means the mask representation of each object does not depend on its category. On the contrary, we propose to leverage object classes to generate semantic and stable masks.

**Diffusion probabilistic model (DPM).** Diffusion models [30] belong to a class of likelihood-based generative models that comprise two processes, namely, the forward diffusion process and the reverse diffusion process. Ho *et al.* [13] first clarified the equivalence of diffusion models and score-based models [31] and proposed a denoising DPM. Later on, further techniques were designed by Dhariwal and Nichol [26, 5] to improve and illustrate the superior performance of diffusion models over GAN [9]. In particular, an additional classifier is trained on noisy images and utilize gradients to guide the sampling process based on the conditioning information. On the contrary, Ho and Salimans [15] argued that a pure generative model could provide guidance without needing a classifier. Inspired by

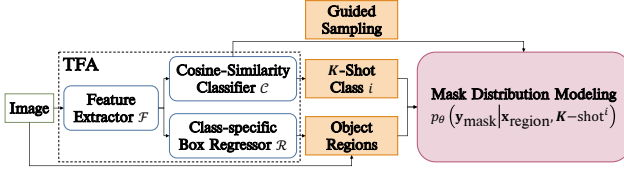


Figure 2. Our MaskDiff is built upon TFA [34] by integrating a mask distribution modeling head and adapting guided sampling to integrate category information into mask generation procedure.

the work of Ho and Salimans [15], we employ classifier-free guided diffusion based mask sampling, in which we use the off-the-shelf cosine classifier from the box-classification head instead of training additional classifiers.

Several research works have studied the adaptation of conditional DPMs to downstream tasks including super-resolution [14, 28], text-to-image synthesis [17, 10], image inpainting [22, 4], and image segmentation [2]. To the best of our knowledge, our proposed MaskDiff is the first work that adapts conditional DPM to FSIS.

### 3. Methodology

#### 3.1. Problem formulation

In few-shot learning [16], we have a disjoint set of base classes  $\mathbf{C}_{\text{base}}$  which contains a large quantity of training data and a set of novel classes  $\mathbf{C}_{\text{novel}}$  with a limited number of annotated data  $\mathbf{C}_{\text{base}} \cap \mathbf{C}_{\text{novel}} = \emptyset$ . The main objective is to train a model that performs well on the novel classes  $\mathbf{C}_{\text{test}} = \mathbf{C}_{\text{novel}}$  or on both base and novel classes together  $\mathbf{C}_{\text{test}} = \mathbf{C}_{\text{base}} \cup \mathbf{C}_{\text{novel}}$ . Following the steps of few-shot classification, prior works [16, 35] simulate the *episodic-training* methodology which randomly samples a series of episodes  $\mathcal{E} = \{(\mathbf{I}_j^q, \mathcal{S}_j)\}_{j=1}^{|\mathcal{E}|}$  where the  $j$ -th episode is formulated by sampling a support set  $\mathcal{S}_j$  including  $N$  classes from  $\mathbf{C}_{\text{train}} = \mathbf{C}_{\text{base}} \cup \mathbf{C}_{\text{novel}}$  in tandem with  $K$  samples per class ( $N$ -way,  $K$ -shot) and a query image  $\mathbf{I}_j^q$ . The goal of FSIS is not only to localize all the object instances from any query image and classify those objects but also determine their segmentation masks. For all objects in a query image  $\mathbf{I}^q$  that belong to  $\mathbf{C}_{\text{test}}$ , FSIS generates the corresponding labels, bounding boxes, and segmentation masks.

#### 3.2. Motivation

To express the representative of each class, which is regarded as point estimation, a popular mechanism is to choose a single point (usually the mean of  $K$  representation vectors of  $K$  samples). However, the point estimation approach suffers from several obstacles, as follows:

1. **Bias and unreliability.** It is challenging to estimate such a precise representative for each class only by a few samples provided. Due to a significant lack of data, prototype-based techniques compute the mean

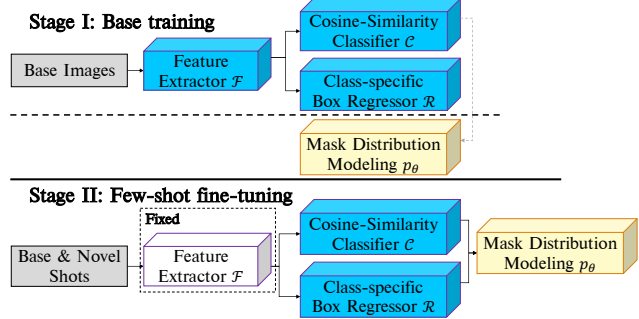


Figure 3. Pipeline of diffusion-based two-stage training. In the first stage, the entire object detector (feature extractor, classifier and box regressor) and the mask distribution modeling head are trained separately on the base classes. In the second stage, the feature extractor is frozen while the cosine classifier, the box regressor, and the mask distribution modeling head are jointly fine-tuned on both base and novel classes. Our mask distribution modeling head is trained based on diffusion (yellow), while the remaining two heads follow the standard object detection training (blue).

of embedded support examples for each class, which is susceptible to noise [1]. We hypothesize that the binary mask representation of each object is sampled from a high-dimensional conditional distribution conditioned on RGB image and  $K$ -shot examples. Thus, a single prototypical vector is insufficient to comprehensively capture diverse levels of semantic information, including object boundaries, poses, or categories.

2. **Spatial information degradation.** Compressing the features of support samples as well as query objects via several pooling operators unavoidably destroys the spatial information of the support images. In addition, the spatial information plays an essential role in delineating objects correctly, and losing spatial features leads to poor detailed segmentation results.

To explicitly solve problems caused by point estimation approaches, we propose to model the conditional distribution of a binary mask, which is conditioned on RGB image and  $K$ -shot support samples. Assuming the mask representation of each object follows a mixture of Gaussian distribution, it is difficult to precisely estimate the distribution in regions of low data density in terms of few-shot learning tasks [31]. Following data augmentation methods, our strategy is to perturb data points with sufficient Gaussian noise, thus increases the population of low data density regions and improves the effectiveness of modeling distribution, especially in limited data regions.

#### 3.3. Proposed MaskDiff method

**Overview.** Figure 2 illustrates the architecture of our MaskDiff, adapted from TFA [34], which is a two-stage object detection architecture. We build a mask distribution modeling head on top of TFA. Unlike class-agnostic mask predictor [8] or prototype-based mask head [7], we

propose to model the conditional distribution of a binary mask conditioned on an instance region and  $K$ -shot samples via conditional DPMs. With regard to denoising architecture of the mask distribution modeling branch, we adapt UNet [29] architecture with attention heads [32] from Guided Diffusion [5]. In particular, the conditioning module consists of the concatenation of a detected object region and  $K$ -shot samples. We empirically found that the permutation of  $K$ -shot does not affect the model’s performance since the encoder-decoder architecture leverages information of each shot independently. Meanwhile, point estimation methods [7, 8] compute the mean features of  $K$ -shot that suffers from bias and unreliability. The detailed denoising architecture is illustrated in Supplementary Material.

**Diffusion-based two-stage training.** Figure 3 visualizes our diffusion-based two-stage training for FSIS. In the first stage, *i.e.*, the base training stage, the network is trained only on the base classes  $\mathbf{C}_{\text{base}}$ . We separately train few-shot object detector heads and estimate the mask distribution. Specifically, the RoI cosine-similarity classifier  $\mathcal{C}$  and the box regressor  $\mathcal{R}$  follow the standard training process while the mask distribution modeling head  $p_{\theta}(\mathbf{y}_{\text{mask}}|\mathbf{x}_{\text{region}}, K\text{-shot}^i)$  is proposed to train based on conditional DPM. The reason is that in this early stage, the box regressor  $\mathcal{R}$  is not stable enough, and it is complicated for probabilistic models to estimate the mask distribution efficiently. Obviously, incorrectly localizing objects leads to extremely unsatisfactory segmentation results.

The second stage, *i.e.*, the few-shot fine-tuning stage, involves freezing the entire feature extractor  $\mathcal{F}$  and jointly fine-tuning prediction heads on a balanced dataset of  $K$  shots for both  $\mathbf{C}_{\text{base}}$  and  $\mathbf{C}_{\text{novel}}$  classes. Likewise, all the prediction heads  $\mathcal{C}$ ,  $\mathcal{R}$ , and  $p_{\theta}$  are fine-tuned.

### 3.4. Instance mask modeling with conditional DPM

Given a FSIS dataset, we extract a dataset of input-output pairs denoted  $\mathcal{D} = \{(\mathbf{x}_{\text{region}}^d, K\text{-shot}; \mathbf{y}_{\text{mask}}^d)\}_{d=1}^{|\mathcal{D}|}$  for modeling the binary mask distribution given object regions and  $K$ -shot information.  $\mathbf{x}_{\text{region}}^d$ ’s are collected by cropping object regions from the RGB images by bounding box locations in the annotations.  $\mathbf{y}_{\text{mask}}^d$ ’s are converted from polygons to binary mask representations at the same location as  $\mathbf{x}_{\text{region}}^d$ ’s. Finally,  $K$ -shot samples of each class are the background removed version of the object region. For simplicity, we denote  $\mathbf{y}$ ,  $\mathbf{x}$ ,  $\mathbf{k}$  to represent binary masks, object regions, and  $K$ -shot guidance, respectively. In this work, we aim to learn the underlying conditional distribution from which a data point representing a binary mask is sampled  $\mathbf{y}_0 \sim q(\mathbf{y}|\mathbf{x}, \mathbf{k})$ . However, we are unable to determine exactly the true distribution. Via diffusion models, we maximize the likelihood  $p_{\theta}(\mathbf{y}_0|\mathbf{x}, \mathbf{k}) = \int p_{\theta}(\mathbf{y}_{0:T}|\mathbf{x}, \mathbf{k}) d\mathbf{y}_{1:T}$  to approximate the true distribution. In the conditional diffusion probabilistic models, two processes are defined, in-

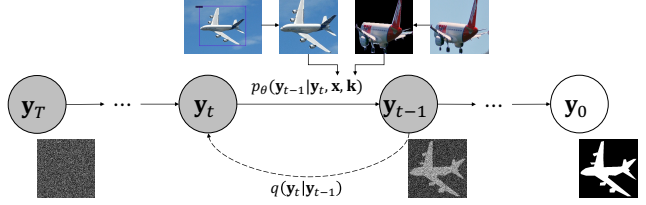


Figure 4. Conditional diffusion model for few-shot binary mask segmentation. The directed graphical model transforms the noise from standard Gaussian distribution to the mask representation of objects through an iterative denoising process. Solid arrows indicate the reverse process while the dashed arrow implies the forward step.  $\mathbf{y}$ ,  $\mathbf{x}$ ,  $\mathbf{k}$  denote binary masks, object regions and removed background version of  $K$ -shot samples, respectively.

cluding the forward and reverse processes (see Fig. 4).

**Forward diffusion process.** The forward diffusion process is defined in which we gradually add a small amount of Gaussian noise to the sample in  $T$  steps, producing a sequence of noisy samples  $\mathbf{y}_1, \dots, \mathbf{y}_T$ , formulated as follows:

$$q(\mathbf{y}_{1:T}|\mathbf{y}_0) = \prod_{t=1}^T q(\mathbf{y}_t|\mathbf{y}_{t-1}), \quad (1)$$

where Gaussian noise is added at each iteration of the forward process as follows:

$$q(\mathbf{y}_t|\mathbf{y}_{t-1}) = \mathcal{N}(\mathbf{y}_t; \sqrt{1 - \beta_t} \mathbf{y}_{t-1}, \beta_t \mathbf{I}). \quad (2)$$

The data sample  $\mathbf{y}_0$  gradually loses its distinguishable features as step  $t$  becomes larger. Eventually, when  $T \rightarrow \infty$ ,  $\mathbf{y}_T$  is equivalent to an isotropic Gaussian distribution. The step sizes are controlled by a variance schedule  $\{\beta_t \in (0, 1)\}_{t=1}^T$ . A nice property of the forward diffusion process is that we can sample  $\mathbf{y}_t$  at any arbitrary time step  $t$  in a closed form using the reparameterization trick. Let  $\alpha_t = 1 - \beta_t$  and  $\bar{\alpha}_t = \prod_{i=1}^T \alpha_i$ , we have:

$$q(\mathbf{y}_t|\mathbf{y}_0) = \mathcal{N}(\mathbf{y}_t; \sqrt{\bar{\alpha}_t} \mathbf{y}_0, (1 - \bar{\alpha}_t) \mathbf{I}). \quad (3)$$

**Reverse diffusion process.** The reverse diffusion process  $p_{\theta}(\mathbf{y}_{0:T}|\mathbf{x}, \mathbf{k})$  is defined as a Markov chain with learned Gaussian transitions beginning with  $p(\mathbf{y}_T) \sim \mathcal{N}(\mathbf{0}, \mathbf{I})$ , which is formulated as follows:

$$p_{\theta}(\mathbf{y}_{0:T}|\mathbf{x}, \mathbf{k}) = p(\mathbf{y}_T) \prod_{t=1}^T p_{\theta}(\mathbf{y}_{t-1}|\mathbf{y}_t, \mathbf{x}, \mathbf{k}), \quad (4)$$

where reverse process steps are performed by taking small Gaussian steps described by:

$$p_{\theta}(\mathbf{y}_{t-1}|\mathbf{y}_t, \mathbf{x}, \mathbf{k}) = \mathcal{N}(\mathbf{y}_{t-1}; \mu_{\theta}(\mathbf{y}_t, \mathbf{x}, \mathbf{k}, t), \Sigma_{\theta}(\mathbf{y}_t, \mathbf{x}, \mathbf{k}, t)). \quad (5)$$

**Diffusion loss.** The conditional diffusion probabilistic model is trained to minimize the cross entropy as the learning objective, which is equivalent to minimize variational upper bound (VUB) (see Supplementary Materials for detailed derivation of loss functions):

$$L_{\text{CE}} \leq \mathbb{E}_{q(\mathbf{y}_{0:T}|\mathbf{x}, \mathbf{k})} \left[ \log \frac{q(\mathbf{y}_{1:T}|\mathbf{y}_0)}{p_{\theta}(\mathbf{y}_{0:T}|\mathbf{x}, \mathbf{k})} \right] = L_{\text{VUB}}. \quad (6)$$

---

**Algorithm 1** Training Procedure

---

**repeat**

$\mathbf{x} \sim q(\mathbf{x})$ ,  $\mathbf{x}$  belongs to class  $i$ ,  $\mathbf{k} = K$  shots of class  $i$

$\mathbf{y}_0 \sim q(\mathbf{y}_0|\mathbf{x}, \mathbf{k})$

$t \sim \text{Uniform}(1, \dots, T)$

$\epsilon \sim \mathcal{N}(\mathbf{0}, \mathbf{I})$

Take gradient descent step on

$$\nabla_{\theta} \|\epsilon - \epsilon_{\theta}(\sqrt{\bar{\alpha}_t} \mathbf{y}_0 + \sqrt{1 - \bar{\alpha}_t} \epsilon, \mathbf{x}, \mathbf{k}, t)\|^2$$

**until** converged

---

To convert each term in the equation to be analytically computable, the objective can be further rewritten to be a combination of several KL-divergence and entropy terms:

$$\begin{aligned} L_{\text{VUB}} = \mathbb{E}_q & \left[ \underbrace{D_{\text{KL}}(q(\mathbf{y}_T|\mathbf{y}_0) \parallel p_{\theta}(\mathbf{y}_T))}_{L_T} \right. \\ & + \sum_{t=1}^{T-1} \underbrace{D_{\text{KL}}(q(\mathbf{y}_t|\mathbf{y}_{t+1}, \mathbf{y}_0) \parallel p_{\theta}(\mathbf{y}_t|\mathbf{y}_{t+1}, \mathbf{x}, \mathbf{k}))}_{L_t} \\ & \left. - \underbrace{\log p_{\theta}(\mathbf{y}_0|\mathbf{y}_1, \mathbf{x}, \mathbf{k})}_{L_0} \right]. \end{aligned} \quad (7)$$

Following the standard training process of DPM [13], the loss term  $L_t$  is parameterized to achieve better training, resulting in a simplified loss:

$$L_t = \mathbb{E}_{\mathbf{y}_0, \epsilon} [\|\epsilon - \epsilon_{\theta}(\sqrt{\bar{\alpha}_t} \mathbf{y}_0 + \sqrt{1 - \bar{\alpha}_t} \epsilon, \mathbf{x}, \mathbf{k}, t)\|^2], \quad (8)$$

where  $\epsilon \sim \mathcal{N}(\mathbf{0}, \mathbf{I})$ . Training procedure is shown in Alg. 1.

**Classifier-free guided mask sampling.** In contrast to class-agnostic mask segmentation [8, 25], we integrate category knowledge into binary mask generation. It is known that the mask representation of each object depends upon not only its boundary but also its category. Hence, the mask distribution modeling head is able to be aware of discriminative properties of objects. In other words, the diffusion model explicitly controls binary masks via object labels.

Inspired by the derivation of score-based models [31], the distribution  $p(\mathbf{y}_t|\mathbf{x}, \mathbf{k}, \mathbf{c})$  has the score  $\nabla \log p(\mathbf{y}_t|\mathbf{x}, \mathbf{k}, \mathbf{c})$ , where  $\mathbf{c}$  is a one-hot vector indicating the category of the instance object, which is naturally achieved by classification branch. Via Bayes' rule, we derive the following equivalent form:

$$\begin{aligned} \nabla \log p(\mathbf{y}_t|\mathbf{x}, \mathbf{k}, \mathbf{c}) &= \nabla \log \left( \frac{p(\mathbf{y}_t|\mathbf{x}, \mathbf{k}) p(\mathbf{c}|\mathbf{y}_t, \mathbf{x}, \mathbf{k})}{p(\mathbf{c}|\mathbf{x}, \mathbf{k})} \right) \\ &= \underbrace{\nabla \log p(\mathbf{y}_t|\mathbf{x}, \mathbf{k})}_{\text{guidance-agnostic score}} + \underbrace{\nabla \log p(\mathbf{c}|\mathbf{y}_t, \mathbf{x}, \mathbf{k})}_{\text{adversarial gradient}}. \end{aligned} \quad (9)$$

Classifier guidance [5] adjusts the adversarial gradient of the noisy classifier by a  $\omega$  hyper-parameter term to introduce fine-grained control to either encourage or dissuade the model from accepting the conditioning information.

---

**Algorithm 2** Inference Procedure with Guided Sampling

---

$\mathbf{y}_T \sim \mathcal{N}(\mathbf{0}, \mathbf{I})$

**for**  $t = T, \dots, 1$  **do**

$\epsilon \sim \mathcal{N}(\mathbf{0}, \mathbf{I})$  if  $t > 1$ , otherwise  $\epsilon \leftarrow \mathbf{0}$

$\hat{\epsilon}_{\theta} \leftarrow \omega \epsilon_{\theta}(\mathbf{y}_t, \mathbf{x}, \mathbf{k}, \mathbf{c}, t) + (1 - \omega) \epsilon_{\theta}(\mathbf{y}_t, \mathbf{x}, \mathbf{k}, t)$

$\mathbf{y}_{t-1} \leftarrow \frac{1}{\sqrt{\alpha_t}} \left( \mathbf{y}_t - \frac{\beta_t}{\sqrt{1 - \alpha_t}} \hat{\epsilon}_{\theta} \right) + \sigma_t \epsilon$

**end for**

**return**  $\mathbf{y}_0$

---

The score function is thus described as follows:

$$\nabla \log p(\mathbf{y}_t|\mathbf{x}, \mathbf{k}, \mathbf{c}) = \nabla \log p(\mathbf{y}_t|\mathbf{x}, \mathbf{k}) + \omega \nabla \log p(\mathbf{c}|\mathbf{y}_t, \mathbf{x}, \mathbf{k}). \quad (10)$$

Inspired by classifier-free guidance [15], we substitute the adversarial gradient term in Eq. 9 into Eq. 10, resulting:

$$\nabla \log p(\mathbf{y}_t|\mathbf{x}, \mathbf{k}, \mathbf{c}) = \underbrace{\omega \nabla \log p(\mathbf{y}_t|\mathbf{x}, \mathbf{k}, \mathbf{c})}_{\text{guidance-specific score}} + \underbrace{(1 - \omega) \nabla \log p(\mathbf{y}_t|\mathbf{x}, \mathbf{k})}_{\text{guidance-agnostic score}}. \quad (11)$$

As  $\nabla \log p(\mathbf{y}_t|\mathbf{x}, \mathbf{k}, \mathbf{c}) = -\frac{1}{\sqrt{1 - \alpha_t}} \epsilon_{\theta}(\mathbf{y}_t, \mathbf{x}, \mathbf{k}, \mathbf{c}, t)$  (see Supplementary Materials for more details), we have the equivalent form:

$$\hat{\epsilon}_{\theta}(\mathbf{y}_t, \mathbf{x}, \mathbf{k}, \mathbf{c}, t) = \underbrace{\omega \epsilon_{\theta}(\mathbf{y}_t, \mathbf{x}, \mathbf{k}, \mathbf{c}, t)}_{\text{guidance-specific score}} + \underbrace{(1 - \omega) \epsilon_{\theta}(\mathbf{y}_t, \mathbf{x}, \mathbf{k}, t)}_{\text{guidance-agnostic score}}. \quad (12)$$

The inference procedure with guided sampling is shown in Alg. 2. When  $\omega > 1$ , the diffusion model not only favors the guidance-specific score function over the guidance-agnostic one but also moves away from it. Along with producing samples that accurately match the conditioning information, this also reduces sample variety and makes generated masks more stable. Following Ho *et al.* [15], we set  $\omega = 5$  to obtain the most individual sample fidelity.

## 4. Experiments

### 4.1. Implementation details

Our MaskDiff was implemented using the Detectron2 library. The used backbone architecture was a ResNet50 [12] and we utilized Feature Pyramid Network (FPN) [19] for path aggregation block. The mask distribution modeling head was implemented using Guided Diffusion [5, 15] with 1,000 reverse steps. In the base training stage, similar to TFA [34], object detector heads were trained using SGD with a learning rate of 0.02, momentum of 0.9, and weight decay of  $10^{-4}$ . The mask distribution modeling head was trained using AdamW with a learning rate of  $10^{-4}$ ,  $\beta_1 = 0.9$  and  $\beta_2 = 0.999$ . We also used an exponential moving average (EMA) rate of 0.9999. Object regions, binary masks and  $K$ -shot guidance were all resized to  $128 \times 128$  for training the mask distribution modeling head. In the few-shot fine-tuning stage, the entire network including object detector heads and the mask distribution modeling head

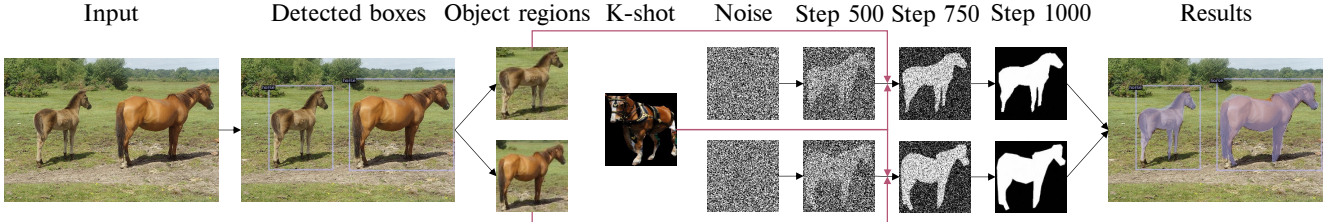


Figure 5. Inference example of our MaskDiff when training and inference on one-shot setting for the COCO novel classes. More successful and failure cases of our method can be found in Supplementary Materials.

Table 1. FSOD and FSIS performance on COCO dataset for both base and novel classes (COCO-All). MaskDiff outperforms state-of-the-art methods. The best performance is marked in boldface.

Shots	Method	Published	Object Detection						Instance Segmentation					
			All Classes		Base Classes		Novel Classes		All Classes		Base Classes		Novel Classes	
			AP	AP <sub>50</sub>	AP	AP <sub>50</sub>	AP	AP <sub>50</sub>	AP	AP <sub>50</sub>	AP	AP <sub>50</sub>	AP	AP <sub>50</sub>
1	MRCN+ft-full [11]	ICCV 2017	10.21	21.58	17.63	26.32	0.74	2.33	9.88	19.25	15.57	24.18	0.64	2.14
	MTFA [8]	CVPR 2021	24.32	39.64	31.73	51.49	2.10	4.07	22.98	37.48	29.85	48.64	2.34	3.99
	iMTFA [8]	CVPR 2021	21.67	31.55	27.81	40.11	3.23	5.89	20.13	30.64	25.9	39.28	2.81	4.72
	iFS-RCNN [25]	CVPR 2022	31.19	52.83	40.08	71.14	4.54	10.29	28.45	46.72	36.35	63.11	3.95	7.89
	<b>MaskDiff (Ours)</b>	-	<b>32.59</b>	<b>54.61</b>	<b>41.23</b>	<b>72.85</b>	<b>5.26</b>	<b>11.35</b>	<b>29.42</b>	<b>48.37</b>	<b>37.59</b>	<b>64.26</b>	<b>4.85</b>	<b>8.73</b>
5	MRCN+ft-full [11]	ICCV 2017	12.31	23.69	19.43	28.12	1.15	2.09	11.28	22.36	17.89	26.78	1.17	2.58
	MTFA [8]	CVPR 2021	26.39	41.52	33.11	51.49	6.22	11.63	25.07	39.95	31.29	49.55	6.38	11.14
	iMTFA [8]	CVPR 2021	19.62	28.06	24.13	33.69	6.07	11.15	18.22	27.10	22.56	33.25	5.19	8.65
	iFS-RCNN [25]	CVPR 2022	32.52	54.30	40.06	71.19	9.91	19.24	29.89	48.22	36.33	62.81	8.80	15.73
	<b>MaskDiff (Ours)</b>	-	<b>33.45</b>	<b>56.19</b>	<b>41.51</b>	<b>72.28</b>	<b>10.49</b>	<b>21.07</b>	<b>30.48</b>	<b>50.35</b>	<b>38.12</b>	<b>64.36</b>	<b>9.43</b>	<b>17.12</b>
10	MRCN+ft-full [11]	ICCV 2017	12.44	24.39	20.57	29.72	2.33	5.64	12.15	23.29	18.08	27.53	1.86	4.25
	MTFA [8]	CVPR 2021	27.44	42.84	33.83	52.04	8.28	15.25	25.97	41.28	31.84	50.17	8.36	14.58
	iMTFA [8]	CVPR 2021	19.26	27.49	23.36	32.41	6.97	12.72	17.87	26.46	21.87	32.01	5.88	9.81
	iFS-RCNN [25]	CVPR 2022	33.02	56.15	40.05	69.84	12.55	25.97	30.41	49.54	36.32	63.29	10.06	19.72
	<b>MaskDiff (Ours)</b>	-	<b>35.21</b>	<b>59.80</b>	<b>42.17</b>	<b>72.36</b>	<b>14.04</b>	<b>28.33</b>	<b>31.89</b>	<b>52.15</b>	<b>38.55</b>	<b>66.48</b>	<b>11.84</b>	<b>21.27</b>

Table 2. FSOD and FSIS performance on only COCO novel classes (COCO-Novel). MaskDiff outperforms state-of-the-art methods. Results on other K-shot are described on Supplementary Materials.

Shots	Method	Detection		Segmentation	
		AP	AP <sub>50</sub>	AP	AP <sub>50</sub>
10	MRCN+ft-full [11]	2.52	5.78	1.93	4.68
	Meta-RCNN [35]	5.60	14.20	4.40	10.60
	MTFA [8]	8.52	15.53	8.40	14.62
	iMTFA [8]	7.14	12.91	5.94	9.96
	iFS-RCNN [25]	11.27	22.15	10.22	20.61
	<b>MaskDiff (Ours)</b>	<b>12.18</b>	<b>23.61</b>	<b>11.01</b>	<b>21.58</b>

were jointly trained with the same configuration as training the mask distribution modeling head in the first stage. In the final step of the denoising process, we set the threshold of noisy binary masks to 0.5 to separate 0 and 1 values. All variants of MaskDiff were trained with a batch size of 8 on a single NVIDIA RTX 3090 GPU.

## 4.2. Experimental settings

Following the standard FSIS evaluation [34, 8, 25], we evaluated MaskDiff on COCO [20], VOC2007 [6], and VOC2012 [6] datasets. 80 classes of COCO were split as suggested by Kang *et al.* [16]. 20 classes that intersect with

Table 3. FSIS performance on COCO2VOC. MaskDiff outperforms state-of-the-art methods. The authors of FGN [7] reported only AP50 results of one-shot.

Shots	Method	Detection		Segmentation	
		AP	AP <sub>50</sub>	AP	AP <sub>50</sub>
1	FGN [7]	-	-	30.80	-
	MTFA [8]	9.99	21.68	9.51	19.28
	iMTFA [8]	11.47	22.41	8.57	16.32
	<b>MaskDiff (Ours)</b>	<b>24.15</b>	<b>38.57</b>	<b>22.73</b>	<b>37.59</b>

Table 4. Additional experiments on COCO-20<sup>i</sup> dataset (*i* denotes the number of shots). We use the same training and evaluation protocol of compared methods [24, 33] for a fair evaluation.

Method	Detection		Segmentation	
	#1	#5	#1	#5
FAPIS [24]	21.20	23.60	19.00	21.20
DTN [33]	23.80	25.30	21.50	23.40
<b>MaskDiff (Ours)</b>	<b>26.48</b>	<b>28.17</b>	<b>24.73</b>	<b>26.25</b>

VOC were used as novel classes, whereas the remaining 60 classes were used as base classes. The union of COCO training set (80k images) and COCO validation set (35k images) was utilized for training, while the remaining 5k images served as the test set. We also combined validation sets of VOC2007 and VOC2012 only for testing methods.

We compared the performance of  $K = 1, 5, 10$  shots per

novel class. We repeated all tests 10 times with  $K$  random samples per class to limit the influence of outliers caused by the random selection of  $K$  shots and report the mean result. Our FSIS assessment approach is identical to that of few-shot object detection (FSOD) [34]. Crucially, segmentation results of different runs are not unique since the masks sampled in the inference depend on random factors ( $y_T \sim \mathcal{N}(\mathbf{0}, \mathbf{I})$ ,  $\epsilon \sim \mathcal{N}(\mathbf{0}, \mathbf{I})$ ). To provide a stable and reliable evaluation procedure of generative-based models, we propose a simple yet effective evaluation method inspired by TFA [34]. With a model trained on specific  $K$  shots, we performed inference for multiple runs on different random seeds to obtain averages and confidence intervals. We observed that 10 runs are comparatively reliable and stable for evaluation reports. To sum up, we trained models for 10 runs on different samples of training shots, and with each trained model, we tested on 10 different random seeds.

### 4.3. Comparison with state-of-the-art methods

**Results on both COCO base and novel classes (COCO-All).** In this experiment, we aim to predict all 80 COCO classes and report the standard evaluation metrics, including mAP and AP50. Following the newly introduced evaluation process of Ganea *et al.* [8], we report the performance of the base and novel classes independently as well as all classes. We compared our MaskDiff against state-of-the-art methods, such as MTFA [8], iMTFA [8], iFS-RCNN [25], and a fully-converged Mask R-CNN model fine-tuned on the novel classes (MRCN+ft-full) [11].

Results in Table 1 show that MaskDiff consistently outperforms state-of-the-art methods on both FSOD and FSIS tasks on both base and novel classes for all numbers of provided shots. This implies MaskDiff has ability to adapt to novel classes while embracing performance in base classes.

Especially, MaskDiff outperforms MTFA [8] and iMTFA [8], the two SOTA methods utilizing TFA [34] as the core of developed networks, with significant margins on the COCO dataset. Particularly, compared with MTFA [8], for 10 shots, our performance of FSIS gains are about +3.5 on new classes and +7 on base classes. Likewise, our MaskDiff also dramatically outperforms iMTFA [8] with gains of +6 on novel classes and +17 on base classes. Modeling mask distribution via DPM shows more effectiveness than conventional methods and gains large performance on learning both existing and new categories on limited data.

**Results on only COCO novel classes (COCO-Novel).** Table 2 reports our results on only COCO novel classes, in which we compared MaskDiff against state-of-the-art FSIS methods (*e.g.*, Meta-RCNN [35], MTFA [8], iMTFA [8], iFS-RCNN [25], and MRCN+ft-full [11]). Experimental results demonstrated the superior performance of MaskDiff on both detection and segmentation tasks consistently on all  $K$ -shots. MaskDiff surpasses the recent iFS-RCNN [25]

Table 5. Our ablation study on COCO-Novel dataset. MaskDiff with classifier-free guided mask sampling and diffusion-based two-stage training strategy achieves the best performance. Removing the guidance, the effectiveness of the network witnesses a gradual decrease, while not using the proposed training leads to a drastic drop in AP. Results on other  $K$ -shot are described on Supplementary Materials.

Shots	MaskDiff		Detection		Segmentation	
	Guided	Two-Stage Training	AP	AP <sub>50</sub>	AP	AP <sub>50</sub>
10	✗	✗	10.59	20.96	9.68	18.83
	✓	✗	10.86	21.55	10.02	19.48
	✗	✓	12.05	23.32	10.76	20.63
	✓	✓	12.18	23.61	11.01	21.58

Table 6. We train our MaskDiff on a specific set of training samples and perform inference on 10 different random seeds. Then, we compute the mean and standard deviation (std) AP of those runs. Clearly, MaskDiff with guided sampling not only outperforms the one without guidance but also is more stable (std is less). Qualitative results of classifier-free guided mask sampling can be seen in Supplementary Materials.

Shots	MaskDiff	Segmentation	
		AP	AP <sub>50</sub>
1	w/o guided sampling	$6.04 \pm 0.09$	$12.29 \pm 0.12$
	<b>w/ guided sampling</b>	$6.23 \pm \mathbf{0.07}$	$12.47 \pm \mathbf{0.08}$
5	w/o guided sampling	$9.71 \pm 0.06$	$20.51 \pm 0.10$
	<b>w/ guided sampling</b>	$10.14 \pm \mathbf{0.05}$	$20.65 \pm \mathbf{0.06}$
10	w/o guided sampling	$10.77 \pm 0.06$	$20.68 \pm 0.09$
	<b>w/ guided sampling</b>	$11.04 \pm \mathbf{0.04}$	$21.60 \pm \mathbf{0.06}$

Table 7. Stability of FSIS performance on COCO-All dataset. MaskDiff is the most stable method with smallest standard deviation of AP. The best performance is marked in boldface. Results on other  $K$ -shot are described on Supplementary Materials.

Shots	Method	All Classes	Base Classes	Novel Classes
1	MRCN+ft-full [11]	$9.88 \pm 0.31$	$15.57 \pm 0.30$	$0.64 \pm 0.26$
	MTFA [8]	$22.98 \pm 0.24$	$29.85 \pm 0.35$	$2.34 \pm 0.31$
	iMTFA [8]	$20.13 \pm 0.28$	$25.90 \pm 0.32$	$2.81 \pm 0.37$
	iFS-RCNN [25]	$28.45 \pm 0.12$	$36.35 \pm 0.01$	$3.95 \pm 0.48$
MaskDiff (Ours)		$29.42 \pm \mathbf{0.09}$	$37.59 \pm \mathbf{0.0093}$	$4.85 \pm \mathbf{0.24}$

and drastically outperforms other methods by a large margin in terms of AP. This indicates that our proposal is better than previous strategies including episodic-training (Meta-RCNN [35]), class-specific mask predictor (MTFA [8]) and class-agnostic one (iMTFA [8], iFS-RCNN [25]).

**Cross-dataset COCO2VOC evaluation.** To additionally investigate the ability to learn new categories, we compared MaskDiff with some state-of-the-art FSIS methods (*e.g.*, FGN [7], MTFA [8], and iMTFA [8]) on cross-dataset COCO2VOC setting. Methods were trained on COCO dataset and evaluated on VOC dataset. We reported public results provided by authors, which are only in one-shot setting ( $K = 1$ ). Table 3 shows that our MaskDiff transcends cutting-edge methods on cross-dataset evaluation. More importantly, our mask distribution modeling approach outperforms point estimation one (FGN [7]).

**Qualitative evaluation.** We trained and performed inference of MaskDiff on one-shot setting ( $K = 1$ ) on the COCO novel classes. The results are demonstrated in Fig. 5. The top row illustrates a successful case, while a failure case is shown in the bottom row. Regarding the failure one, a white “dog” is classified as “bear” and imperfectly segmented. The other dog is also imprecisely delineated despite being correctly categorized. Apparently, misclassification and inadequate information from training samples lead to poor segmentation results.

**Additional comparison.** Our work uses a different training and evaluation protocol than FAPIS [24] and DTN [33], two SOTA methods in FSIS. Unlike these works, our work follows TFA’s training and evaluation strategy [34], which is more standard and common. For a fair comparison, we additionally compared our MaskDiff using the same evaluation protocol as these works. As seen in Table 4, our MaskDiff significantly outperforms these two methods by a large margin.

#### 4.4. Ablation study

**Effectiveness of two-stage training strategy.** We aim to evaluate the effectiveness of the proposed two-stage training strategy consisting of base training and few-shot finetuning. In base training, we first train object detector and then K-shot mask modeling on base images. In finetuning stage, we jointly train both object detector heads and our mask distribution modeling head on balanced base and novel classes. We compared our approach with the common approach using only few-shot fine-tuning stage. Particularly, we exclude the first stage training on base images (*i.e.*, base training) and utilize only the second stage. In early steps, the object detector cannot localize and classify the objects precisely. Given unsatisfactory localized object regions, the mask distribution modeling head is much more difficult to train, leading to generate not good segmentation masks. Table 5 shows a considerable collapse in results.

**Significance of classifier-free guided mask sampling.** We studied the effectiveness as well as stability of classifier-free guided mask sampling by comparing the performance MaskDiff with and without classifier-free guided mask sampling. From Table 5, we conclude that classifier-free guided mask sampling boosts the performance of FSIS. Furthermore, we evaluated the standard deviation of testing results on 10 different random seeds when running on a specific samples of training shots. In Table 6, we can see that the standard deviation of MaskDiff with guidance over 10 different random seeds is less than that of without guidance. In other words, the classifier-free guided mask sampling makes the mask distribution modeling head more stable.

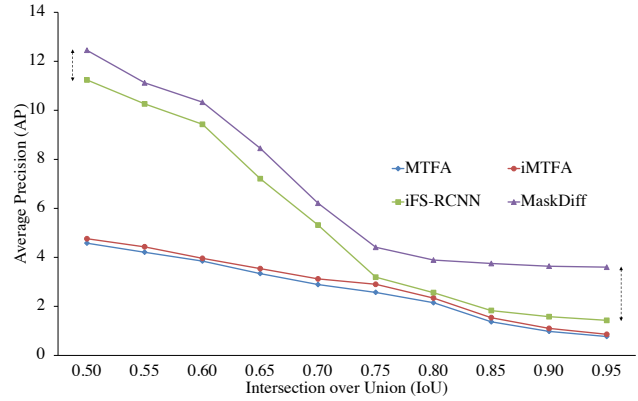


Figure 6. MaskDiff preserves spatial information, especially at detailed levels. We compare the performance of MaskDiff with state-of-the-art methods in one-shot instance segmentation at different IoU thresholds. MaskDiff outperforms other methods with large margins at high IoU thresholds, which indicates its ability to segment objects more precisely.

#### 4.5. Further analysis

In this section, we demonstrate that our proposed MaskDiff improves the stability of performance in FSIS. In addition, we show that MaskDiff is able to delineate objects correctly at the detailed level as the mask distribution modeling head utilizes direct RGB object regions instead of pooled features as in prior works [11, 7, 8, 25].

**Stability analysis.** The performance of various methods has been generally evaluated based on the evaluation protocol proposed by Wang *et al.* [34]. In particular, a certain model is trained on a different set of training samples and is evaluated on the same test set to report the mean result. We further computed the standard deviation of different runs and compared the stability with state-of-the-art methods. Table 7 shows that our MaskDiff achieves the highest performance and the lowest standard deviation in terms of AP, indicating that MaskDiff is the most stable and robust to different  $K$  training samples.

**Spatial information preservation.** Most conventional FSIS methods leverage pooled object features and feed them into Fully Convolutional Network (FCN) [21] to generate binary masks. However, passing through several pooling layers leads to a severe collapse in spatial information, especially the detailed one. By directly utilizing object regions from input images to generate binary masks, our MaskDiff can embrace comprehensive spatial details and induce precise delineation. In Fig. 6, we visualize the line graph representing AP from 0.50 to 0.95 with step size 0.05 to illustrate the changes in the performance of FSIS methods when the IoU requirement rises. Our MaskDiff surpasses cutting-edge methods especially at high IoU thresholds.

## 5. Conclusion

In this paper, we presented the first mask distribution modeling approach for FSIS and designed a novel method dubbed MaskDiff. We adapted conditional DPM to model binary mask distribution conditioned on RGB object regions and  $K$ -shot samples. Furthermore, we leveraged the off-the-shelf classifier branch to guide the mask sampling procedure with the category information. Experimental results demonstrated that our proposed method achieves state-of-the-art results whilst being more stable than existing methods. In the future, we aim to model the distribution of all object categories, bounding boxes, and binary masks in a unified approach.

## References

- [1] Kelsey Allen, Evan Shelhamer, Hanul Shin, and Joshua Tenenbaum. Infinite mixture prototypes for few-shot learning. In *International Conference on Machine Learning*, pages 232–241, 2019. 3
- [2] Dmitry Baranckuk, Andrey Voynov, Ivan Rubachev, Valentin Khrulkov, and Artem Babenko. Label-efficient semantic segmentation with diffusion models. In *International Conference on Learning Representations*, 2022. 3
- [3] Daniel Bolya, Chong Zhou, Fanyi Xiao, and Yong Jae Lee. Yolact: Real-time instance segmentation. In *Proceedings of the IEEE/CVF International Conference on Computer Vision (ICCV)*, October 2019. 1
- [4] Hyungjin Chung, Byeongsu Sim, and Jong Chul Ye. Come-closer-diffuse-faster: Accelerating conditional diffusion models for inverse problems through stochastic contraction. In *Proceedings of the IEEE/CVF Conference on Computer Vision and Pattern Recognition (CVPR)*, June 2022. 3
- [5] Prafulla Dhariwal and Alexander Nichol. Diffusion models beat gans on image synthesis. In *Advances in Neural Information Processing Systems*, volume 34, pages 8780–8794, 2021. 2, 4, 5
- [6] Mark Everingham, Luc Van Gool, Christopher K. I. Williams, John M. Winn, and Andrew Zisserman. The pascal visual object classes (voc) challenge. *International Journal of Computer Vision*, 88:303–338, 2010. 6
- [7] Zhibo Fan, Jin-Gang Yu, Zhihao Liang, Jiarong Ou, Changxin Gao, Gui-Song Xia, and Yuanqing Li. Fgn: Fully guided network for few-shot instance segmentation. In *Proceedings of the IEEE/CVF Conference on Computer Vision and Pattern Recognition (CVPR)*, June 2020. 1, 2, 3, 4, 6, 7, 8
- [8] Dan Andrei Ganea, Bas Boom, and Ronald Poppe. Incremental few-shot instance segmentation. In *Proceedings of the IEEE/CVF Conference on Computer Vision and Pattern Recognition (CVPR)*, pages 1185–1194, June 2021. 1, 2, 3, 4, 5, 6, 7, 8
- [9] Ian Goodfellow, Jean Pouget-Abadie, Mehdi Mirza, Bing Xu, David Warde-Farley, Sherjil Ozair, Aaron Courville, and Yoshua Bengio. Generative adversarial nets. In *Advances in Neural Information Processing Systems*, volume 27, 2014. 2
- [10] Shuyang Gu, Dong Chen, Jianmin Bao, Fang Wen, Bo Zhang, Dongdong Chen, Lu Yuan, and Baining Guo. Vector quantized diffusion model for text-to-image synthesis. In *Proceedings of the IEEE/CVF Conference on Computer Vision and Pattern Recognition (CVPR)*, June 2022. 3
- [11] Kaiming He, Georgia Gkioxari, Piotr Dollar, and Ross Girshick. Mask r-cnn. In *Proceedings of the IEEE International Conference on Computer Vision (ICCV)*, Oct 2017. 1, 2, 6, 7, 8
- [12] Kaiming He, Xiangyu Zhang, Shaoqing Ren, and Jian Sun. Deep residual learning for image recognition. In *Proceedings of the IEEE Conference on Computer Vision and Pattern Recognition (CVPR)*, June 2016. 5
- [13] Jonathan Ho, Ajay Jain, and Pieter Abbeel. Denoising diffusion probabilistic models. In *Advances in Neural Information Processing Systems*, volume 33, pages 6840–6851, 2020. 2, 5
- [14] Jonathan Ho, Chitwan Saharia, William Chan, David J. Fleet, Mohammad Norouzi, and Tim Salimans. Cascaded diffusion models for high fidelity image generation. *Journal of Machine Learning Research*, 23(47):1–33, 2022. 3
- [15] Jonathan Ho and Tim Salimans. Classifier-free diffusion guidance. In *NeurIPS Workshop on Deep Generative Models and Downstream Applications*, 2021. 2, 3, 5
- [16] Bingyi Kang, Zhuang Liu, Xin Wang, Fisher Yu, Jiashi Feng, and Trevor Darrell. Few-shot object detection via feature reweighting. In *Proceedings of the IEEE/CVF International Conference on Computer Vision (ICCV)*, October 2019. 3, 6
- [17] Gwanghyun Kim, Taesung Kwon, and Jong Chul Ye. Diffusionclip: Text-guided diffusion models for robust image manipulation. In *Proceedings of the IEEE/CVF Conference on Computer Vision and Pattern Recognition (CVPR)*, June 2022. 3
- [18] Trung-Nghia Le, Yubo Cao, Tan-Cong Nguyen, Minh-Quan Le, Khanh-Duy Nguyen, Thanh-Toan Do, Minh-Triet Tran, and Tam V. Nguyen. Camouflaged instance segmentation in-the-wild: Dataset, method, and benchmark suite. *IEEE Transactions on Image Processing*, 31:287–300, 2022. 1
- [19] Tsung-Yi Lin, Piotr Dollar, Ross Girshick, Kaiming He, Bharath Hariharan, and Serge Belongie. Feature pyramid networks for object detection. In *Proceedings of the IEEE Conference on Computer Vision and Pattern Recognition (CVPR)*, July 2017. 5
- [20] Tsung-Yi Lin, Michael Maire, Serge J. Belongie, James Hays, Pietro Perona, Deva Ramanan, Piotr Dollár, and C. Lawrence Zitnick. Microsoft coco: Common objects in context. In *Proceedings of European Conference on Computer Vision*, 2014. 6
- [21] Jonathan Long, Evan Shelhamer, and Trevor Darrell. Fully convolutional networks for semantic segmentation. In *2015 IEEE Conference on Computer Vision and Pattern Recognition (CVPR)*, pages 3431–3440, 2015. 8
- [22] Andreas Lugmayr, Martin Danelljan, Andres Romero, Fisher Yu, Radu Timofte, and Luc Van Gool. Repaint: Inpainting using denoising diffusion probabilistic models. In *Proceedings of the IEEE/CVF Conference on Computer Vision and Pattern Recognition (CVPR)*, June 2022. 3

[23] C. Michaelis, I. Ustyuzhaninov, M. Bethge, and A. S. Ecker. One-shot instance segmentation. *arXiv*, 2018. 2

[24] Khoi Nguyen and Sinisa Todorovic. Fapis: A few-shot anchor-free part-based instance segmenter. In *Proceedings of the IEEE/CVF Conference on Computer Vision and Pattern Recognition (CVPR)*, pages 11099–11108, June 2021. 2, 6, 8

[25] Khoi Nguyen and Sinisa Todorovic. ifs-rnn: An incremental few-shot instance segmenter. In *Proceedings of the IEEE/CVF Conference on Computer Vision and Pattern Recognition (CVPR)*, pages 7010–7019, June 2022. 2, 5, 6, 7, 8

[26] Alexander Quinn Nichol and Prafulla Dhariwal. Improved denoising diffusion probabilistic models. In *Proceedings of International Conference on Machine Learning*, volume 139, pages 8162–8171, 18–24 Jul 2021. 2

[27] Shaoqing Ren, Kaiming He, Ross Girshick, and Jian Sun. Faster r-cnn: Towards real-time object detection with region proposal networks. In *Advances in Neural Information Processing Systems*, volume 28, 2015. 2

[28] Robin Rombach, Andreas Blattmann, Dominik Lorenz, Patrick Esser, and Björn Ommer. High-resolution image synthesis with latent diffusion models. In *Proceedings of the IEEE/CVF Conference on Computer Vision and Pattern Recognition (CVPR)*, June 2022. 3

[29] Olaf Ronneberger, Philipp Fischer, and Thomas Brox. U-net: Convolutional networks for biomedical image segmentation. In *Medical Image Computing and Computer-Assisted Intervention (MICCAI)*, pages 234–241, 2015. 4

[30] Jascha Sohl-Dickstein, Eric Weiss, Niru Maheswaranathan, and Surya Ganguli. Deep unsupervised learning using nonequilibrium thermodynamics. In *Proceedings of International Conference on Machine Learning*, volume 37, pages 2256–2265, 07–09 Jul 2015. 2

[31] Yang Song and Stefano Ermon. Generative modeling by estimating gradients of the data distribution. In *Advances in Neural Information Processing Systems*, volume 32, 2019. 2, 3, 5

[32] Ashish Vaswani, Noam Shazeer, Niki Parmar, Jakob Uszkoreit, Llion Jones, Aidan N Gomez, Łukasz Kaiser, and Illia Polosukhin. Attention is all you need. In *Advances in Neural Information Processing Systems*, volume 30. Curran Associates, Inc., 2017. 4

[33] Haochen Wang, Jie Liu, Yongtuo Liu, Subhransu Maji, Jan-Jakob Sonke, and Efstratios Gavves. Dynamic transformer for few-shot instance segmentation. In *ACM International Conference on Multimedia*, page 2969–2977, 2022. 2, 6, 8

[34] Xin Wang, Thomas Huang, Joseph Gonzalez, Trevor Darrell, and Fisher Yu. Frustratingly simple few-shot object detection. In *Proceedings of International Conference on Machine Learning*, volume 119, pages 9919–9928, 13–18 Jul 2020. 2, 3, 5, 6, 7, 8

[35] Xiaopeng Yan, Ziliang Chen, Anni Xu, Xiaoxi Wang, Xiaodan Liang, and Liang Lin. Meta r-cnn: Towards general solver for instance-level low-shot learning. In *Proceedings of the IEEE International Conference on Computer Vision*, pages 9577–9586, 2019. 2, 3, 6, 7